


Article

Multi-Frequency GPR Data Fusion through a Joint Sliding Window and Wavelet Transform-Weighting Method for Top-Coal Structure Detection

Zenglun Guan and Wanli Liu * 

School of Mechatronic Engineering, China University of Mining and Technology, Xuzhou 221116, China; db19050013b4cx@cumt.edu.cn

* Correspondence: 4830@cumt.edu.cn; Tel.: +86-516-83590707

Abstract: Top-coal structure detection is an important basis for realizing effective mining in fully mechanized cave faces. However, the top-coal structure is very complex and often contains multi-layer gangues, which seriously influence the level of effective mining. For these reasons, this paper proposes a novel multi-frequency ground-penetrating radar (GPR) data-fusing method through a joint sliding window and wavelet transform weighting method to accurately detect the top-coal structure. It possesses the advantages of both high resolution and great detection depth, and it can also integrate multi-frequency GPR data into one composite profile to interpret the internal structure information of top coal in detail. The detection procedure is implemented following several steps: First of all, the multi-frequency GPR data are preprocessed and aligned through a band-pass filter and a zero offset elimination method to establish their spatial correspondences. Secondly, the proposed method is used to determine the time-varying weight values of each frequency GPR signal according to the wavelet energy proportion within the sliding window; also, the edge detection algorithm is introduced to improve the fusion efficiency of the wavelet transform so as to realize the effective fusion of the multi-frequency GPR data. Thirdly, a reflection intensity model of multi-frequency GPR signals traveling in the top-coal is established by using the stratified identification method, and then, the detailed top-coal structure can be inversely interpreted. Finally, the quantitative evaluation criteria, information entropy (*IE*), space–frequency (*SF*) and Laplacian gradient (*LG*), are used to evaluate the multi-frequency GPR data fusion’s effectiveness in laboratory and field environments. The experimental results show that, compared with the genetic, time-varying and wavelet transform fusion method, the fusion performance of the presented method possesses higher values in the *IE*, *SF* and *LG* evaluation criteria, and it also has both the merits of high resolution and great detection depth.

Keywords: multi-frequency GPR; data fusion; top-coal structure detection; wavelet transform; sliding window



Citation: Guan, Z.; Liu, W. Multi-Frequency GPR Data Fusion through a Joint Sliding Window and Wavelet Transform-Weighting Method for Top-Coal Structure Detection. *Appl. Sci.* **2024**, *14*, 2721. <https://doi.org/10.3390/app14072721>

Academic Editor: Roberto Scarpa

Received: 18 February 2024

Revised: 16 March 2024

Accepted: 22 March 2024

Published: 24 March 2024



Copyright: © 2024 by the authors. Licensee MDPI, Basel, Switzerland. This article is an open access article distributed under the terms and conditions of the Creative Commons Attribution (CC BY) license (<https://creativecommons.org/licenses/by/4.0/>).

1. Introduction

Ground-penetrating radar (GPR) is a nondestructive technique used to detect and locate underground targets and interfaces with high efficiency and resolution; it has become one of the most popular tools used in top-coal structure detection in mine engineering [1,2]. Usually, the structure of top coal in mines with fully mechanized cave faces is very complex and usually contains multi-layer gangues, which often seriously affect the effective level of the fully mechanized cave face. The main reason is that the existence of multi-layer gangues in the top coal will lead to the misjudgment or closure of the coal outlet in the mining process and cause the interruption of effective mining. Therefore, it is urgent to accurately detect detailed top-coal internal structure information (including gangue thickness and layers) before effective mining in fully mechanized cave faces [3,4].

Normally, a high-frequency GPR signal can yield high resolution but limited detection depth, while a low-frequency GPR signal possesses deeper detection depth but lower

resolution [5,6]. However, the detection resolution and depth of complex top-coal structures are always limited when using a single-frequency GPR signal, as it is difficult to simultaneously achieve a deep detection depth and high resolution for top-coal structure detection [7,8]. To overcome the above limitations, a multi-frequency GPR data fusion method is proposed to resolve the unavoidable trade-off between resolution and depth. Furthermore, multi-frequency GPR signals fused and displayed into one profile can enhance GPR data interpretation capacity and accuracy, simultaneously reducing the probability of misjudgment in top-coal structure detection [9,10].

Multi-frequency data fusion is a promising technique for enriching effective frequency signals into one profile. Normally, according to the data collection type, it can be classified into three categories: one involves multi-channel GPR antennas placed at one acquisition site, the next involves multi-frequency antennas placed along the same line, and the last one involves the same antenna placed at different locations. Recently, several GPR data fusion methods have been presented and tested by many researchers: Zhao et al. [11] presented an adaptively weighted fusion method for multi-frequency GPR data based on genetic algorithms. Xu et al. [12] presented a fusion method for ground-penetrating radar data acquired at different center frequencies. De Coster et al. [13] proposed a novel physically based method to merge radar data coming from antennas operating in different frequency ranges. Zhao et al. [14] proposed a novel multi-frequency GPR data fusion method based on a time-varying weighting strategy. Shen et al. [15] proposed a joint deconvolution approach to associate single-frequency data with the target function directly. Lu et al. [16] presented an advanced multi-frequency and multi-attribute GPR data fusion approach based on a 2-D wavelet transform, utilizing a dynamic fusion weight scheme derived from an edge detection algorithm. Yue et al. [17] proposed a fusion framework by combining original profiles with the abovementioned three features based on a two-dimensional wavelet transform. Bi et al. [18] applied multi-frequency GPR data fusion with three algorithms that were evaluated and compared with a fused radar profile and by a Laplacian operator. Xiao et al. [19] developed a signal fusion method to extrapolate a high-frequency, high-resolution GPR signal at a greater depth based on a lower-frequency, greater-penetration signal using extrapolation with a deterministic deconvolution algorithm. Wen et al. [20] presented a multi-station fusion detection method for a moving maritime moving target based on a three-dimensional sliding window.

Although the above literature review demonstrates that the existing GPR data fusion methods have achieved some progress in improving GPR detection resolution and depth, the following limitations still exist [21–24]:

- (1) The current research has only used a relatively simple weighting strategy to fuse multi-frequency GPR signals; its biggest drawback is that the high-frequency components of GPS signals are easily diluted and reduced in time-varying fusion local segments.
- (2) Most of the above studies usually fuse all of the profile information of different-frequency GPRs in one static window; it is difficult to keep the smoothness of the transition in a section when merging high-frequency and low-frequency GPR profiles, and thus is not suitable for fusion occasions when the overlaps of GPS signal bandwidths are not good enough.

Currently, the typical data fusion methods for multi-frequency GPR mainly include wavelet transform, Fourier transform, S-transform and principal component transform. Compared with the other methods, the wavelet transform method has good advantages in signal processing and fusion for multi-frequency GPR data, and it is also widely used in the field of data fusion. However, the current research mainly uses a relatively simple weighting strategy to fuse wavelet transform signals; its biggest drawback is that the high-frequency components of the signal are easily diluted, which results in the loss of high-resolution reflection signals. For these reasons, this paper presents a novel multi-frequency GPR data-fusing method via sliding window and wavelet transform weighting joint to accurately detect top-coal structures, integrating the advantages of high- and low-frequency GPR signals. The main contributions of this work are summarized as follows [25–28]:

- (1) A joint sliding window and wavelet transform-weighting method is proposed for multi-frequency GPR data fusion that can integrate multi-frequency GPR signals into one composite profile with higher resolution and greater detection depths.
- (2) A dynamic sliding window is designed to determine the time-varying weight values of each frequency GPR signal according to the wavelet energy proportion within the sliding window.
- (3) A reflection intensity model of multi-frequency GPR signals traveling in the top coal is established, which can be used to identify the interface information between the coal–gangue–rock and can also effectively display the detailed internal structure of top coal in one composite profile.

The overall framework of this work is elaborated in Figure 1. First of all, the spatial correspondences of different frequency GPR data are established based on the data preprocess and spatial alignment. Secondly, the multi-frequency GPR data are fused through a sliding window and wavelet transform-weighting method. Finally, a reflection intensity model of multi-frequency GPR signals is established to recognize the detailed internal structures of the top coal.

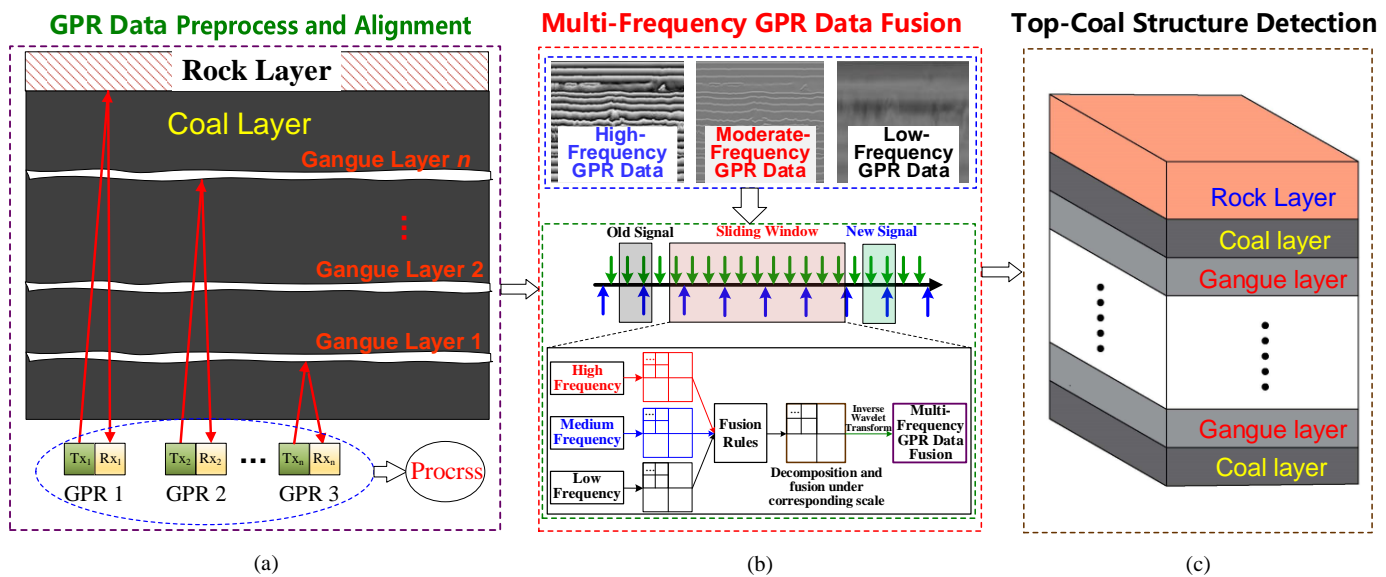


Figure 1. The overall framework of our proposed method. It mainly consists of three stages: (a) GPR Data Preprocessing and Alignment Stage: This is to realize multi-frequency GPR data preprocessing and alignment. (b) Multi-Frequency GPR Data Fusion Stage: This is to integrate the multiple-frequency GPR signals into one representation and enhance the detection information. (c) Top-Coal Structure Detection: This is to interpret the detailed top-coal structure.

2. Materials and Methods

The proposed multi-frequency GPR data fusion method mainly includes 3 modules, GPR data preprocessing and alignment, multi-frequency GPR data fusion and top-coal structure detection, which will be described in detail in the subsequent subsections.

2.1. GPR Data Preprocess and Alignment

As shown in Figure 2, the data preprocessing and alignment process of GPR involves two stages: preprocessing and spatial alignment. Specifically, the preprocess refers to eliminating disturbing information using a pass filter and zero offset elimination algorithm; the spatial alignment refers to performing horizontal and vertical alignment for multi-frequency GPR data.

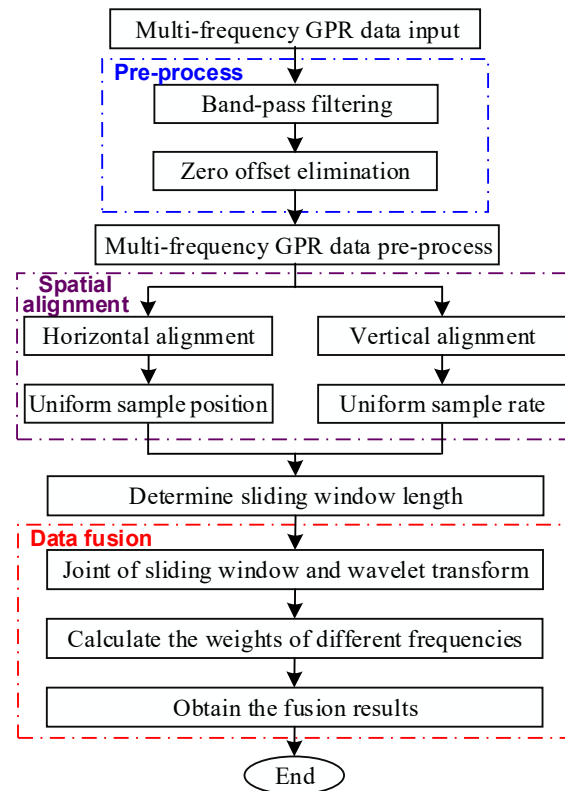


Figure 2. The fusion process of multi-frequency GPR data.

2.1.1. Preprocess

Usually, the different acquired frequency GPR data contain some disturbing noise and random errors. To eliminate the disturbing information and obtain better fusion results, the data preprocess sequences are mainly dealt with using a band-pass filter and zero offset elimination [29,30].

2.1.2. Spatial Alignment

The spatial alignment refers to performing an interpolation of the multi-frequency GPR data and making sure the different frequency data align in the same number of sampling channels. This mainly includes horizontal and vertical spatial alignment; the detailed calculation process is illustrated as follows:

Assume that the GPR sampled data in two different frequencies can be denoted as $X^{m_1}(i, j)$ and $X^{m_2}(i^*, j^*)$, where $i = 1, 2, \dots, m_1, j = 1, 2, \dots, n_1$ and $i^* = 1, 2, \dots, m_2, j^* = 1, 2, \dots, n_2$. Suppose $m_1 > m_2$ and $t_1 < t_2$; thus, the horizontal spatial alignment equation for two different frequencies of GPR data can be calculated as

$$\hat{X}^{m_2}(i, j^*) = \sum_{k=1}^d X^{m_2}\left(\varphi\left(\frac{i(m_2 + d)}{m_1}\right), j^*\right) \text{sinc}(-d) \tag{1}$$

where X^{m_1} and X^{m_2} denote GPR data with different sampled frequencies of m_1 and m_2 ; $\varphi(\cdot)$ denotes the rounding function; and d is a positive integer value.

Similarly, the vertical spatial alignment equation for different frequencies of the GPR data is expressed as

$$\tilde{X}^{m_2}(i, j^*) = \sum_{k=1}^d \hat{X}^{m_2}\left(i, \varphi\left(\frac{j^*(n_1 + d)}{n_1^*}\right) + d\right) \text{sinc}(-d) \tag{2}$$

where $n_1^* = t_1 n_2 / t_2$.

2.2. Multi-Frequency GPR Data Fusion

2.2.1. Data Fusion Method

As shown in Figures 2 and 3, data fusion refers to integrating the multiple-frequency GPR signals into one representation to enhance the detection information and obtain more reliable and detailed results. Suppose there are m different frequencies of GPR signals distributed in the length, L , sliding window and that the sliding window will move ΔL along the time series axis at each step. In the sliding process, the sliding window will contain new GPR signals and remove the oldest GPR signal from the window. The overall optimization model of all GPR signals, $X(t)$, within the sliding window can be calculated by minimizing the cost function of the Markov norm as

$$X^*(t) = \operatorname{argmin}_K \left\{ \sum \|X(t, K)\| - \sum \|X(t, K - \Delta K)\| + \sum \|X(t, K + \Delta K)\| \right\} \quad (3)$$

where $X^*(t)$ represents the overall optimization X model of all radar signals within the sliding window, K , at time t ; $X(t, K)$ denotes the GPR signal data model within the sliding window, L , at time t ; $X(t, K - \Delta K)$ and $X(t, K + \Delta K)$ represent the GPR signal data model within the sliding windows, $K - \Delta K$ and $K + \Delta K$, at time t , respectively; and K and ΔK are the window length and the moving step, respectively.

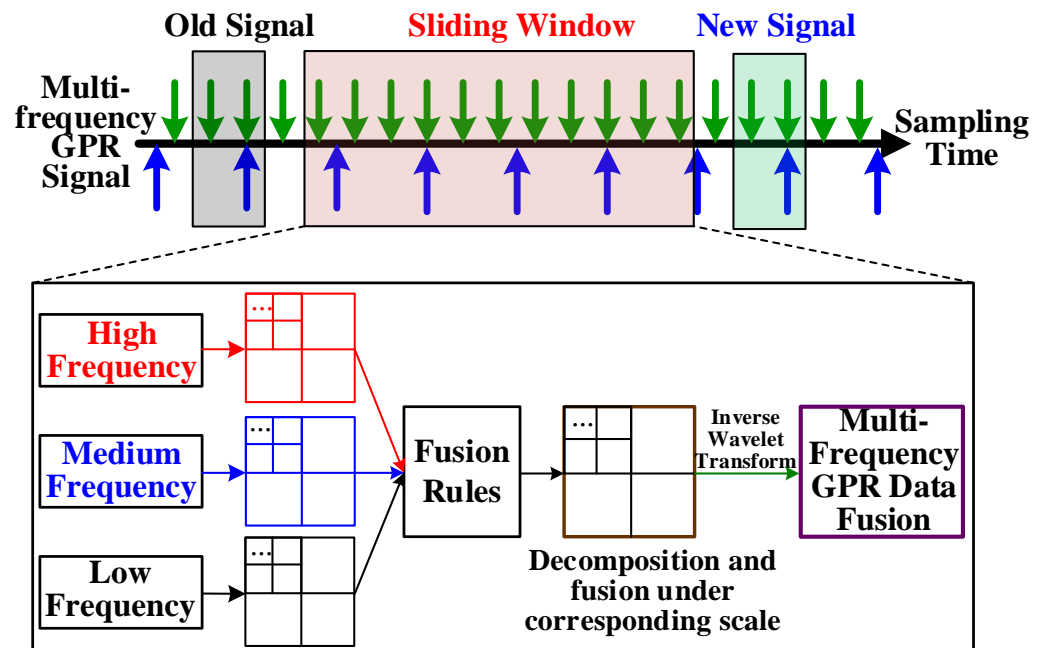


Figure 3. The weighting joint of the sliding window and wavelet transform.

For convenience, assume that the GPR signals within sliding window, L , can be divided into three categories: high-, moderate- and low-frequency GPR signals. Then, the weighted fusion function of each segment frequency signal in the sliding window can be expressed as

$$\tilde{X}(t) = \omega_H X_H^*(t) + \omega_M X_M^*(t) + \omega_L X_L^*(t) \quad (4)$$

where ω_H , ω_M and ω_L denote the weighting factors of high-frequency, moderate-frequency and low-frequency wavelet signals in each segment of the sliding window, the values of ω_H , ω_M and ω_L are within 0 and 1, also, $\omega_H + \omega_M + \omega_L = 1$.

Next, we use the wavelet transform method to calculate the time-varying weight factors of the GPR signals in every frequency band within the sliding window. Suppose that (x, y) is the center point of the sliding window, L ; σ_H , σ_M and σ_L denote the root mean square errors of high-, moderate- and low-frequency GPR signals within the sliding window, respectively, with variances of $D(X_H) = \sigma_H^2$, $D(X_M) = \sigma_M^2$ and $D(X_L) = \sigma_L^2$. To

ensure the $D(X)$ optimization, we should calculate the minimum value of $D(X)$ under the constraint condition $\omega_H + \omega_M + \omega_L = 1$, which is expressed as

$$\begin{cases} \omega_H = \frac{\sum_i^x \sum_j^y (\sigma_H^2(t) W_H^l(i,j))}{\sigma_H^2(t) + \sigma_M^2(t) + \sigma_L^2(t)} \\ \omega_M = \frac{\sum_i^x \sum_j^y (\sigma_M^2(t) W_M^l(i,j))}{\sigma_H^2(t) + \sigma_M^2(t) + \sigma_L^2(t)} \\ \omega_L = \frac{\sum_i^x \sum_j^y (\sigma_L^2(t) W_L^l(i,j))}{\sigma_H^2(t) + \sigma_M^2(t) + \sigma_L^2(t)} \end{cases} \quad (5)$$

where $W_H^l(i, j)$, $W_M^l(i, j)$ and $W_L^l(i, j)$ denote the wavelet function of the high-, moderate- and low-frequency GPR signals within the wavelet decomposition scale, l , and l is the wavelet decomposition scale.

According to the above discussion, we can substitute Equations (3) and (5) into Equation (4) to obtain the multi-frequency GPR fusing result.

The fusing step is summarized in Figure 3; it includes the following steps:

- (1) Obtaining the preprocessing and spatial alignment for the input multi-frequency GPR images.
- (2) Selecting the optimal scale levels to make a wavelet transform for the high-, medium- and low-frequency GPR data, respectively, and obtaining the optimal weighting coefficients of ω_H , ω_M and ω_L based on Equation (5).
- (3) The high-, medium- and low-frequency weighting coefficients are fused according to the multi-frequency fusion rules.
- (4) Inverse wavelet transform, decomposition and fusion under the corresponding scale are conducted to obtain the fusion results of the multi-frequency GPR.

2.2.2. Evaluation Method for Multi-Frequency GPR Data Fusion

To verify the fusion effectiveness of the GPR data, "Information Entropy (IE)", "Space Frequency (SF)" and "Laplacian Gradient (LG)" are employed to quantitatively evaluate the fusing performance of the multi-frequency GPR data.

(1) IE . IE is the basic concept of information theory, which describes the uncertainty of the occurrence of each possible event of a fusion information source. It mainly reflects the average information amount contained in fusion areas; the values of IE strongly correlate with the richness of the information contained in the fusion areas, which can be computed as [31]

$$IE = - \sum_{i=0}^{L-1} p(i) \log_2(p(i)) \quad (6)$$

where $p(i)$ represents the frequency of pixels value at grayscale, i , and L is the total gray value of the image.

(2) SF . SF comes from human visual technology, which represents the overall activity level of an image by coupling the standard scalar quantization of frequency coefficients. Therefore, the larger values of SF imply that the image is clearer. For an $M \times N$ -sized image, assume that each pixel processes the gray value, $F(m, n)$, in position (m, n) ; then, the SF can be calculated as

$$SF = \sqrt{\left(\frac{1}{MN} \sum_{m=1}^M \sum_{n=2}^N (F(m, n) - F(m, n - 1))^2 \right)^2 + \left(\frac{1}{MN} \sum_{n=1}^N \sum_{m=2}^M (F(m, n) - F(m - 1, n))^2 \right)^2} \quad (7)$$

(3) LG . LG refers to the second derivative gradient operator applied to the auto-focus system. In this paper, it will be applied as a clarity indicator to evaluate the fusing results. The LG function of point (x, y) in image $I(x, y)$ can be computed as

$$LG = \frac{\partial^2 I}{\partial x^2} + \frac{\partial^2 I}{\partial y^2} = \frac{1}{n} \times \sum_x \sum_y |I(x + 1, y) + I(x - 1, y) + I(x, y + 1) + I(x, y - 1) - 4I(x, y)| \tag{8}$$

where n is the total number of image pixels. The values of LG are proportional to the image clarity; usually, the clearer of image, the better the detailed features inside the image can be distinguished.

2.3. Top-Coal Structure Detection

2.3.1. GPR Reflection Intensity Model

As shown in Figure 4, assume that all the media in top coal are isotropic and homogeneous and that the top coal contains n gangue layers of thickness L ; the thickness of each coal seam layer is denoted as $L_1, L_3, \dots, L_{2n+1}$, with a relative dielectric constant of $\epsilon_1, \epsilon_3, \dots, \epsilon_{2n+1}$ and a conductivity of $\sigma_2, \sigma_4, \dots, \sigma_{2n}$, while the thickness of each gangue layer is L_2, L_4, \dots, L_{2n} , with a relative dielectric constant of $\epsilon_2, \epsilon_4, \dots, \epsilon_{2n}$ and a conductivity of $\sigma_2, \sigma_4, \dots, \sigma_{2n}$. The relative dielectric constant and conductivity of roof rock are ϵ_{2n+2} and σ_{2n+2} . Suppose that the GPR wave, T_0 , is emitted from a GPR antenna at a distance of L_0 from the coal seam and undergoes reflection and transmission at the interface between the air layer (first layer); assuming an incidence angle of θ_0 and a refraction angle of β_0 , the reflected wave, R_0 , is received through the GPR-receiving antenna. The transmitted wave, T_1 , propagates in the first layer of the medium and undergoes reflection and refraction at the interface between the first and second layers of the medium. Its incidence angle is θ_1 , and the refraction angle is β_1 . The reflected wave, R_1 , will be received by the GPR-receiving antenna. In the same manner, we can obtain the reflected wave, R_{2n+1} , of the $2n + 1$ layer medium and the $2n + 2$ layer medium; then, the total thickness of the coal top is computed based on the two-way travel time of the wave as [32]

$$L = \sum_{i=1}^{2n+1} \frac{v_i t_i \cos \beta_i}{2} \tag{9}$$

where v_i is the propagation speed of GPR waves in the i th layer medium, and t_i is the two-way travel time of electromagnetic waves in the i th layer medium.

The electromagnetic wave intensity of the multi-frequency GPR waves between the air layer and the first layer of the medium can be calculated as

$$P_0 = \frac{P_t G_t}{4\pi(L_0 / \cos \theta_0)^2} \tag{10}$$

where P_t is the initial electromagnetic wave intensity emitted by the GPR, and G_t denotes the transmitting antenna gain.

The reflected wave at the interface between the air layer and the first layer of the medium is obtained by the radar-receiving antenna, and the electromagnetic wave reflection intensity is expressed as

$$R_0 = \frac{P_t G_t G_r \lambda^2 r_{0|1}}{16\pi^2(L_0 / \cos \theta_0)^2} \tag{11}$$

where G_r represents the receiving antenna's gain; λ denotes the wavelength of the electromagnetic wave in the medium; and $r_{0|1}$ represents the reflection coefficient in the first layer interface.

The electromagnetic wave energy of the GPR traveling between the first and second layers of the top coal can be computed as

$$P_1 = \frac{P_t G_t}{4\pi(L_0 / \cos \theta_0 + L_1 / \cos \beta_1)^2} \cdot t_{0|1} e^{-\frac{\alpha_1 L_1}{\cos \beta_1}} \tag{12}$$

where $t_{0|1}$ represents the transmission coefficient of the GPR signal transmitting from the air layer into the first layer; a_1 denotes the attenuation coefficient of the first layer.

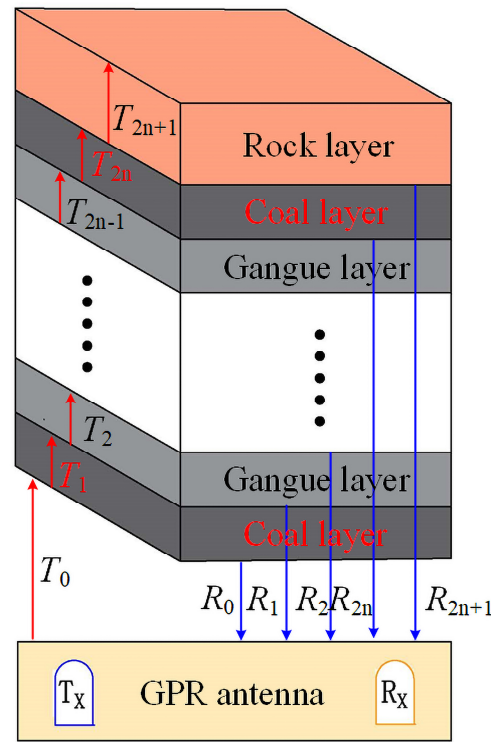


Figure 4. The reflection intensity model of GPR in top coal. It consists of n gangue layers, n coal layers and one rock layer with a total thickness of L ; the travel time of the electromagnetic waves in each coal layer is $t_1, t_3, \dots, t_{2n+1}$, and in each gangue layer is t_2, t_4, \dots, t_{2n} .

The returned electromagnetic wave intensity of the GPR traveling between the first and second layers of the top coal is calculated as

$$R_1 = \frac{P_t G_t G_r \lambda^2 r_{1|2} \cdot t_{0|1} \cdot t_{1|0} \cdot e^{-\alpha_1 \left(\frac{L_1}{\cos \beta_1} + \frac{L_1}{\cos \theta_1} \right)}}{16\pi^2 \left(\frac{L_0}{\cos \theta_0} + \frac{L_0}{\cos \beta_0} + \frac{L_1}{\cos \beta_1} + \frac{L_1}{\cos \theta_1} \right)^2} \tag{13}$$

where $r_{1|2}$ represents the reflection coefficient of the interface between layers 1 and 2 of the medium, $t_{0|1}$ denotes the transmission coefficient of the radar waves entering the first layer of the medium from the air layer, and $t_{1|0}$ represents the transmission coefficient of the GPR wave entering the air layer from the first layer of the medium.

Similarly, the energy expression of the reflecting wave in the interface between the n th and $n + 1$ layers of the media received by the radar antenna can be derived as follows:

$$R_n = \frac{P_t G_t G_r \lambda^2 r_{n|n+1} \cdot \prod_{i=1}^n t_{i-1|i} t_{i|i-1} \cdot e^{-\sum_{i=1}^n \alpha_i \left(\frac{L_i}{\cos \beta_i} + \frac{L_i}{\cos \theta_i} \right)}}{16\pi^2 \left(\sum_{i=0}^n \left(\frac{L_i}{\cos \beta_i} + \frac{L_i}{\cos \theta_i} \right) \right)^2} \tag{14}$$

where $r_{n|n+1}$ represents the reflection coefficient of the interface between the n and $n + 1$ layers of the medium, $t_{i-1|i}$ represents the transmission coefficient of radar waves from the $i - 1$ layer into the i -layer medium, L_i denotes the i -layer medium thickness, β_i represents the transmission angle of the GPR wave from $i - 1$ to the i -layer medium, θ_i represents the incidence angle of the GPR wave from the $i + 1$ layer medium into the i -layer medium, α_i

represents the attenuation coefficient of the i -layer medium, $r_{n|n+1} \cdot \prod_{i=1}^n t_{i-1|i} t_{i|i-1}$ represents the reflection and refraction attenuation of each layer interface, and $e^{-\sum_{i=1}^n \alpha_i (\frac{L_i}{\cos \beta_i} + \frac{L_i}{\cos \theta_i})}$ is the attenuation of radar waves by each layer of media.

2.3.2. Top-Coal Structure Stratification Detection

During the GPR electromagnetic wave transmission in the complex top-coal structure, its transmitting path will be changed at the different dielectric constant interfaces. According to this characteristic, the relationship between the reflecting intensity, R , and the dielectric constant, ϵ , can be computed as follows [33]:

$$\sqrt{\epsilon_{n+1}} = \sqrt{\epsilon_n} \frac{1 - \left(\frac{A_1}{A_0}\right)^2 + \sum_{i=1}^n R_i \frac{A_{i+1}}{A_m} + \frac{A_n}{A_m}}{1 - \left(\frac{A_1}{A_0}\right)^2 + \sum_{i=1}^n R_i \frac{A_{i+1}}{A_0} - \frac{A_n}{A_0}} \tag{15}$$

where A is the amplitude of the GPR reflection wave, A_0 is the GPR reflection wave amplitude in the air layer, and the reflection energy of R is provided in Equation (14).

According to Equation (15), the dielectric constant of each layer in the top coal can be determined; and then, the stratification structure of each layer in the top coal can be recognized based on the dielectric constant value.

3. Results and Discussion

To estimate the effectiveness of our presented method, we conducted both laboratory and field experiments in different conditions. We further performed both qualitative and quantitative analyses based on the data from the multi-frequency GPR signals.

3.1. Laboratory Tests

As shown in Figure 5, from top to bottom, the constructed top-coal structure in laboratory conditions mainly includes a rock layer, a coal layer, a gangue layer and a coal layer; two groups of GPR central frequencies (900 MHz and 1500 MHz) were selected to verify the GPR data fusion effectiveness in the laboratory environment. In the experiments, we separately used two frequencies for the GPR antenna to detect the top-coal structure; subsequently, preprocessing and spatial alignment were carried out to deal with the multi-frequency GPR data. Assume that the time window of each frequency GPR profile was uniformly set to 15 ns, and the number of sampling points was 512 channels. For the sake of simple analysis, we selected 400 trace data of multi-frequency GPR to verify the fusion effectiveness.

The experimental results are provided in Figure 6. We can see that the detection accuracy and image resolution of the 1500 MHz GPR profile in Figure 6a are more accurate than that of the 900 MHz GPR profile in Figure 6b with a range of 0~7.5 ns, while the 1500 MHz GPR profile penetration distance is limited to about 7.5 ns; when the transmitting time is greater than 7.5 ns, the reflection signal is almost invisible in the GPR profile. Conversely, the 900 MHz GPR profile still has a reflection signal between 7.5 ns and 11 ns. To effectively combine the high detection resolution of the 1500 MHz GPR data and the large penetration depth of the 900 MHz GPR data, we used our proposed method to fuse the 1500 MHz and 900 MHz frequency GPR data; the experimental results are provided in Figure 6c. We can see that the fusion results of the 900 MHz and 1500 MHz GPRs not only possess high-resolution characteristics of high frequency in a range of 0~7.5 ns but also have a large penetration depth of low frequency in a range of 7.5~15 ns.

To quantitatively evaluate the multi-frequency GPR data fusion effectiveness in a laboratory environment, our proposed method was compared with the genetic [11], time-varying [14] and wavelet transform [16] fusion methods based on the *IE*, *SF* and *LG* evaluation criteria. The comparison results are provided in Table 1; it can be seen that the low-frequency GPR profile (900 MHz) has a higher value of *IE* and *LG* due to its greater penetration depth, while the high frequency (1500 MHz) possesses a higher value of *SF* because of its higher resolution. The fusion results for the 900 MHz and 1500 MHz GPR data using our proposed method possess the best performance. Compared with the genetic, time-varying and wavelet transform fusion methods, the fusion results for the *IE*, *SF* and *LG* evaluation criteria improved by “12.74%, 11.46% and 11.97%”; “13.59%, 11.47% and 11.96%”; and “12.77%, 8.51% and 10.64%”, respectively. Furthermore, the above experimental results prove that the multi-frequency GPR data fused by our proposed method possess both the merits of high-frequency GPR data—higher-resolution and low-frequency data and greater detection depth—further proving our presented method to be feasible and effective.

Table 1. The comparison results of our proposed method with the genetic, time-varying and wavelet transform methods using 900 MHz and 1500 MHz GPR data.

Item	900 MH	1500 MH	Our Proposed Method	Genetic Method	Time-Varying Method	Wavelet Transform Method
<i>IE</i>	6.74	5.24	7.85	6.85	6.95	6.91
<i>SF</i>	26.33	28.21	43.57	37.65	38.57	38.36
<i>LG</i>	0.37	0.31	0.47	0.41	0.43	0.42

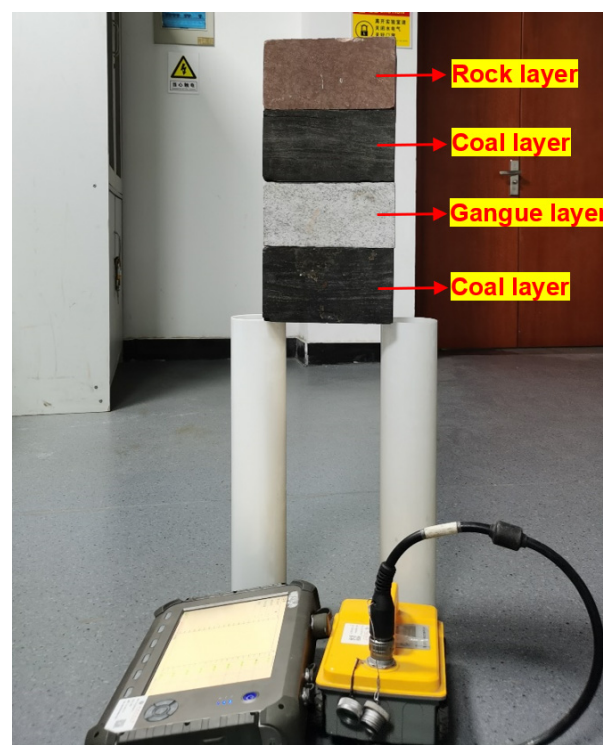


Figure 5. The complex top-coal structure model. It consists of four different layer structures, from top to bottom: a rock layer, a coal layer, a gangue layer and a coal layer; also, every layer has a different dielectric constant and conductivity.

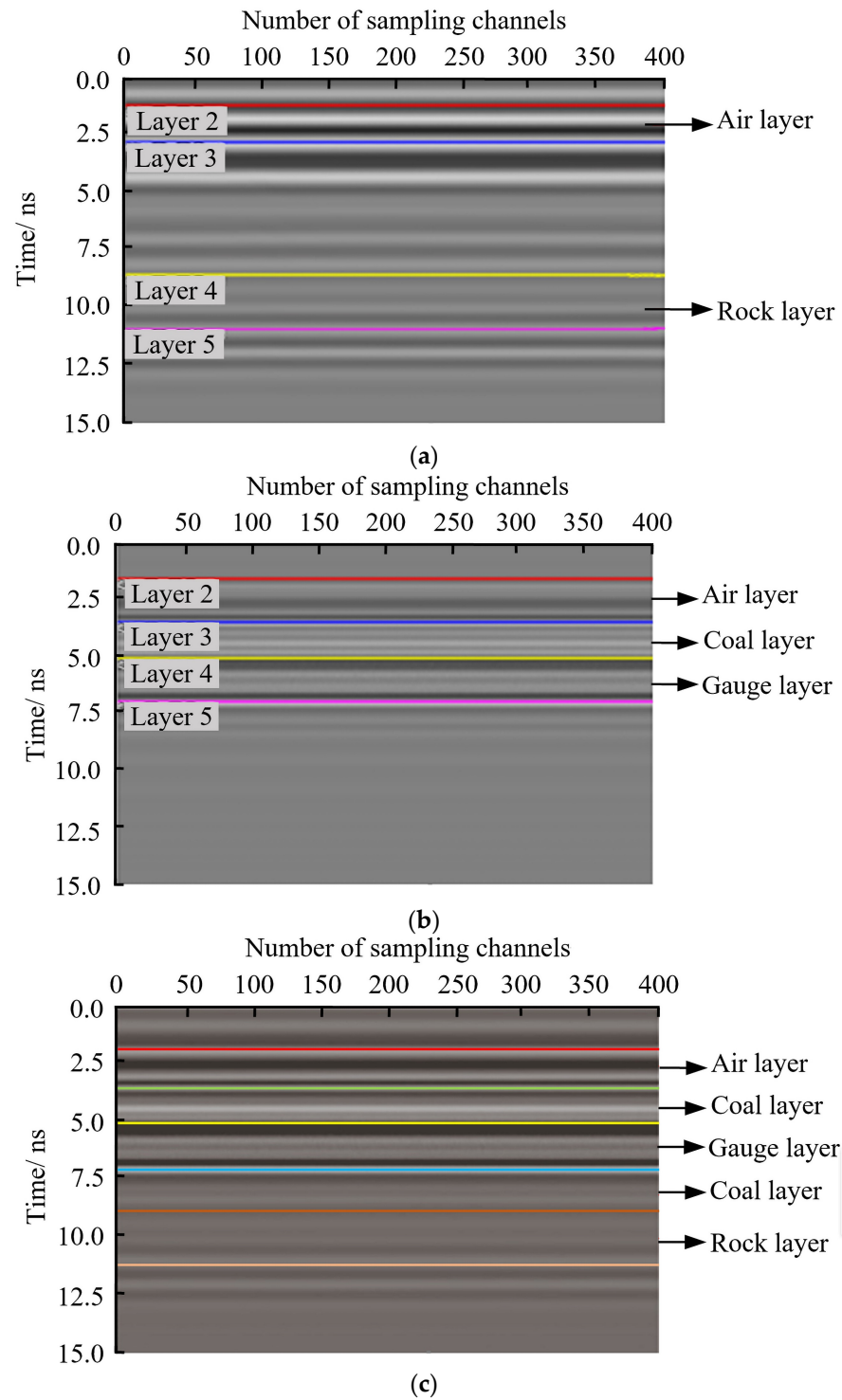


Figure 6. Multi-frequency GPR data fusion results for top coal in laboratory environments: (a) 900 MHz GPR profile; (b) 1500 MHz GPR profile; (c) 900 MHz and 1500 MHz fused profile.

3.2. Field Tests

We also carried out field tests on the fully mechanized mine cave face. A detailed structure of the top coal is provided in Figure 7; the average thickness of the top coal is 12.36 m; the maximum number of gangue layers in the top coal is five; and the thickness of the gangue layer is from 0.1 to 4 m.

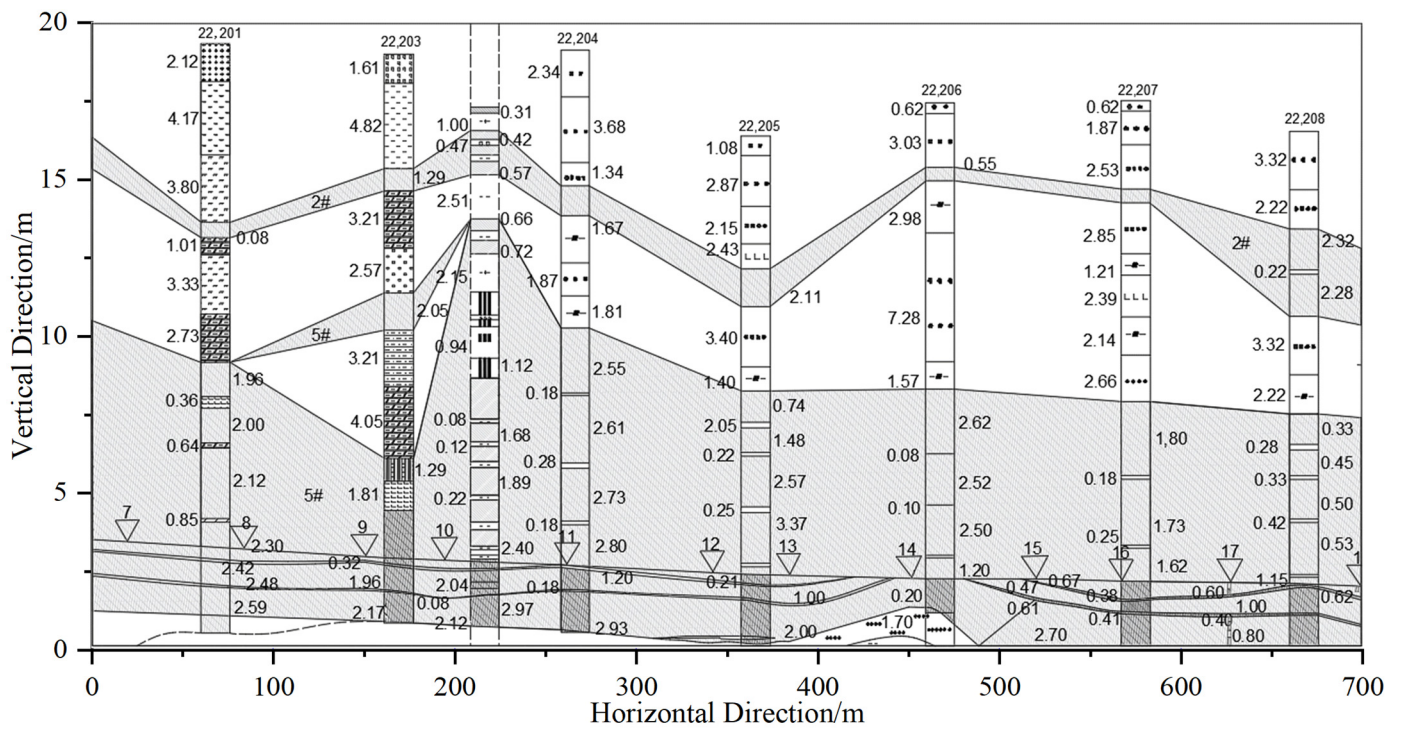


Figure 7. The structure of top coal in a fully mechanized cave face, where the horizontal axis denotes the horizontal direction of the mine face, and the vertical axis represents the thickness of the top coal.

In the field tests, we selected two groups of GPR central frequencies (100 MHz and 270 MHz) based on the thickness of the top coal (its average thickness was about 12 m) to detect the top-coal structure (see Figure 8). The GPR antenna was placed on a moving vehicle; in this experiment, the static measurement mode was adopted for multi-frequency GPR data acquisition, and 30 sampling channels of GPR signals were selected to analyze the data fusion performance. Also, we chose three representative borehole locations to verify our proposed method’s effectiveness. Note that the detailed structures of the top coal in the borehole location were obtained via manual operation.

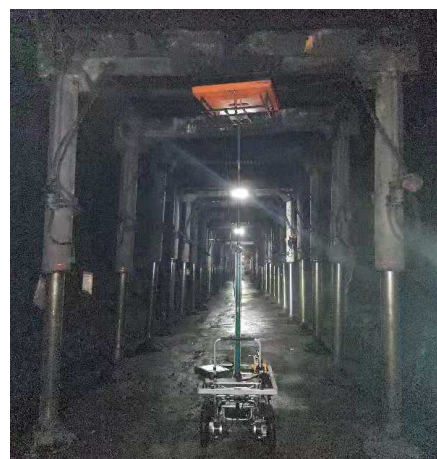


Figure 8. The layout of the GPR in field tests.

The test results are provided in Figure 9, where the horizontal axis denotes the number of sampling channels, and the vertical axis represents the GPR signals’ propagation time. Figure 9a,b denote the 100 MHz and 270 MHz GPR waveform accumulation profile, and Figure 9c represents the GPR-fused waveform accumulation profile. We can see that the

detection distance of the 100 MHz frequency GPR is relatively larger than the 270 MHz frequency GPR; in a range of 150–300 ns, the echo intensity and image resolution were higher. Conversely, the echo intensity and image resolution of the 270 MHz frequency GPR were outstanding, in a range of 0–150 ns, while for a range greater than 150 ns, the detection affection became worse. Figure 9c shows that the fused results not only possessed the merits of higher detection resolution in a range of 0–150 ns but also had larger penetration depth in a range of 150–300 ns.

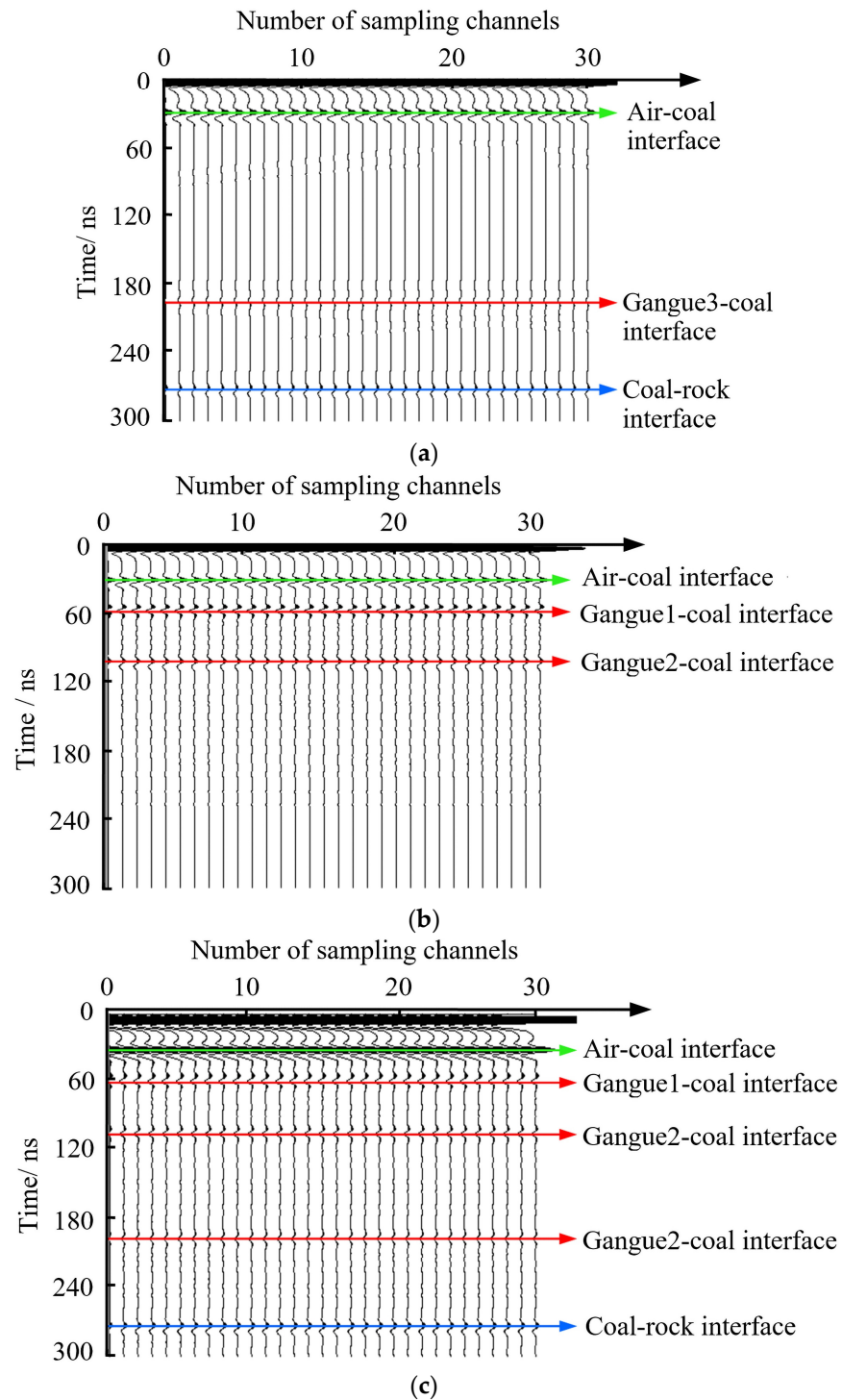


Figure 9. Multi-frequency GPR data fusion results for top coal in field environments: (a) 100 MHz GPR waveform accumulation profile; (b) 270 MHz GPR waveform accumulation profile; (c) 100 MHz and 270 MHz GPR fused waveform accumulation profile.

Similar to Table 1, we also compared the genetic, time-varying and wavelet transform fusion methods with our proposed method to evaluate multi-frequency GPR data fusion's effectiveness in a field environment. The comparison results are provided in Table 2; we can see that the fusion results for the 100 MHz and 270 MHz GPR data using our proposed method possess the best performance; compared with the genetic, time-varying and wavelet transform fusion methods, the fusion results for the *IE*, *SF* and *LG* evaluation criterion improved by "15.72%, 44.89% and 19.11%"; "10.77%, 9.47% and 12.13%"; and "14.08%, 7.04% and 12.61%", respectively. Moreover, the experimental results prove that multi-frequency GPR data fusing can increase the information content and profile clarity, and it also possesses both the merits of high-frequency GPR signals: higher-resolution and low-frequency signals and greater detection depth.

Table 2. The comparison results for our proposed method with the genetic, time-varying and wavelet transform methods using 100 MHz and 270 MHz GPR data.

Item	100 MH	270 MH	Our Proposed Method	Genetic Method	Time-Varying Method	Wavelet Transform Method
<i>IE</i>	10.11	7.86	13.87	11.69	12.72	11.22
<i>SF</i>	39.49	42.32	64.27	57.35	59.18	56.47
<i>LG</i>	0.55	0.46	0.71	0.61	0.68	0.62

4. Conclusions

To realize the accurate detection of complex top-coal structures, we propose a novel multi-frequency GPR data-fusing method using a joint sliding window and wavelet transform-weighting method. It possesses both the merits of high resolution and great detection depth and has the ability to integrate multi-frequency GPR data into one composite profile to interpret the internal structure information of top coal in detail. Also, we developed an edge detection algorithm to improve the fusion efficiency of the wavelet transform so as to realize the effective fusion of multi-frequency GPR data. Furthermore, we established a reflection intensity model of multi-frequency GPR signals traveling in top coal and interpreted the detailed top coal structure. The experimental results prove that, compared with the genetic method, the time-varying method and the wavelet transform method, the fusion results for our proposed method in terms of the *IE*, *SF* and *LG* evaluation criteria have improved by "12.74%, 11.46% and 11.97%"; "13.59%, 11.47% and 11.96%"; and "12.77%, 8.51% and 10.64%" and "15.72%, 44.89% and 19.11%"; "10.77%, 9.47% and 12.13%"; and "14.08%, 7.04% and 12.61%" in laboratory and field environments, respectively. Moreover, our method can also accurately interpret the internal structure of top coal.

Although the proposed multi-frequency GPR data fusion method possesses many merits in detecting top-coal structures, there are still some issues that should be addressed in further research: (1) In fusion experiments, we only selected two kinds of GPR frequencies to evaluate fusion effectiveness; thus, in future work, multiple frequencies of GPR will be considered and compared. (2) More fusion performance assessments and evaluations of multi-frequency GPR data fusion will be conducted for further applications to deal with more challenging scenarios.

Author Contributions: Writing—original draft, Z.G.; writing—review and editing, W.L.; All authors have read and agreed to the published version of the manuscript.

Funding: This research was funded by the Industry and Information Technology Development Program of Foundation Reconstruction and Manufacturing Industry High-Quality Development of China (TC220A04W-1-167Z) and the National Natural Science Foundation of China (52274161).

Institutional Review Board Statement: Not applicable.

Informed Consent Statement: Not applicable.

Data Availability Statement: The data are contained within this article.

Acknowledgments: The authors would like to thank the editors and the reviewers of this journal.

Conflicts of Interest: The authors declare no conflicts of interest.

References

1. Primusz, P.; Abdelsamei, E.; Ali, A.M.; Sipos, G.; Fi, I.; Herceg, A.; Tóth, C. Assessment of In Situ Compactness and Air Void Content of New Asphalt Layers Using Ground-Penetrating Radar Measurements. *Appl. Sci.* **2024**, *14*, 614. [\[CrossRef\]](#)
2. Temlioglu, E.; Erer, I. A novel convolutional autoencoder-based clutter removal method for buried threat detection in ground-penetrating radar. *IEEE Trans. Geosci. Remote Sens.* **2022**, *60*, 5103313. [\[CrossRef\]](#)
3. Duan, H.; Zhao, L.; Yang, H.; Zhang, Y.; Xia, H. Development of 3D top coal caving angle model for fully mechanized extra-thick coal seam mining. *Int. J. Min. Sci. Technol.* **2022**, *32*, 1145–1152. [\[CrossRef\]](#)
4. Yang, Y.; Zhang, Y.; Zeng, Q. Research on coal gangue recognition based on multi-layer time domain feature processing and recognition features cross-optimal fusion. *Measurement* **2022**, *204*, 112169. [\[CrossRef\]](#)
5. Comite, D.; Ahmad, F.; Amin, M.G.; Dogaru, T. Forward-looking ground-penetrating radar: Subsurface target imaging and detection: A review. *IEEE Geosci. Remote Sens. Mag.* **2021**, *9*, 173–190. [\[CrossRef\]](#)
6. Leibowitz, C.; Weiss, A.J. Underground Cavity Detection through Group Dispersion of a GPR Signal. *Remote Sens.* **2022**, *14*, 4808. [\[CrossRef\]](#)
7. Yang, J.; Ruan, K.; Gao, J.; Yang, S.; Zhang, L. Pavement distress detection using three-dimension ground penetrating radar and deep learning. *Appl. Sci.* **2022**, *12*, 5738. [\[CrossRef\]](#)
8. Zhang, L.; Zhang, S.; Deng, Z.; Ling, T. Geological detection of hard rocks by GPR and signal time-frequency characteristics analysis in urban underground trenchless construction. *Meas. Sci. Technol.* **2024**, *35*, 045406. [\[CrossRef\]](#)
9. Jin, Y.; Duan, Y. A new method for abnormal underground rocks identification using ground penetrating radar. *Measurement* **2020**, *149*, 106988. [\[CrossRef\]](#)
10. Hao, T.; Jing, L.; He, W. An Automated GPR Signal Denoising Scheme Based on Mode Decomposition and Principal Component Analysis. *IEEE Geosci. Remote Sens. Lett.* **2023**, *20*, 3500105. [\[CrossRef\]](#)
11. Zhao, W.K.; Yuan, L.; Forte, E.; Lu, G.Z.; Tian, G.; Pipan, M. Multi-frequency GPR data fusion with genetic algorithms for archaeological prospection. *Remote Sens.* **2021**, *13*, 2804. [\[CrossRef\]](#)
12. Xu, X.L.; Li, J.P.; Qiao, X.; Fang, G. Fusion of multiple time-domain GPR datasets of different center frequencies. *Near Surf. Geophys.* **2019**, *17*, 141–150. [\[CrossRef\]](#)
13. De Coster, A.; Lambot, S. Fusion of multifrequency GPR data freed from antenna effects. *IEEE J. Sel. Top. Appl. Earth Observ. Remote Sens.* **2018**, *11*, 664–674. [\[CrossRef\]](#)
14. Zhao, W.K.; Lu, G.Z. A novel multifrequency GPR data fusion algorithm based on time-varying weighting strategy. *IEEE Geosci. Remote Sens. Lett.* **2022**, *19*, 3510104. [\[CrossRef\]](#)
15. Shen, H.L.; Tian, G.; Tao, C.H.; Wang, H.C.; Fang, J.W. Multi-frequency data fusion via joint weighted deconvolution for resolution enhancement. *J. Appl. Geophys.* **2022**, *203*, 104702. [\[CrossRef\]](#)
16. Lu, G.Z.; Zhao, W.K.; Forte, E.; Tian, G.; Li, Y.; Pipan, M. Multi-frequency and multi-attribute GPR data fusion based on 2-D wavelet transform. *Measurement* **2020**, *166*, 108243. [\[CrossRef\]](#)
17. Yue, G.; Du, Y.; Liu, C.; Guo, S.; Li, Y.; Gao, Q. Road subsurface distress recognition method using multiattribute feature fusion with ground penetrating radar. *Int. J. Pavement Eng.* **2023**, *24*, 2037591. [\[CrossRef\]](#)
18. Bi, W.; Zhao, Y.; Shen, R.; Li, B.; Hu, S.; Ge, S. Multi-frequency GPR data fusion and its application in NDT. *NDT E Int.* **2020**, *115*, 102289. [\[CrossRef\]](#)
19. Xiao, J.; Liu, L. Permafrost subgrade condition assessment using extrapolation by deterministic deconvolution on multifrequency GPR data acquired along the Qinghai-Tibet railway. *IEEE J. Sel. Top. Appl. Earth Observ. Remote Sens.* **2016**, *9*, 83–90. [\[CrossRef\]](#)
20. Wen, H.; Li, Y.; Duan, C.; Zhang, J.; Li, N.; Wu, T. Multi-radar data fusion for maritime moving target detection based on three-dimensional sliding window. *Int. J. Remote Sens.* **2023**, *44*, 646–665. [\[CrossRef\]](#)
21. Zhao, Y.; Ling, C.; Zhang, K.; Gao, Y.; Sun, B.; Wang, X. Detection of hidden mining-induced ground fissures via unmanned aerial vehicle infrared system and ground-penetrating radar. *Int. J. Min. Sci. Technol.* **2022**, *160*, 105254. [\[CrossRef\]](#)
22. Li, Y.; Wang, J.; Chen, Y.; Wang, Z.; Wang, J. Overlying strata movement with ground penetrating radar detection in close-multiple coal seams mining. *Int. J. Distrib. Sens. Netw.* **2019**, *15*, 1–8. [\[CrossRef\]](#)
23. Daniels, D.J.; Van Verre, W.; Podd, F.; Peyton, A.J. Antenna Design Considerations for Ground Penetrating Radar Landmine Detection. *J. Appl. Geophys.* **2022**, *70*, 4273–4286. [\[CrossRef\]](#)
24. Wang, S.; Leng, Z.; Zhang, Z.; Sui, X. Automatic asphalt layer interface detection and thickness determination from ground-penetrating radar data. *Constr. Build. Mater.* **2022**, *357*, 129434. [\[CrossRef\]](#)
25. Zhang, L.; Ling, T.H.; Yu, B.; Huang, F.; Zhang, S. Intensive interferences processing for GPR signal based on the wavelet transform and F-K filtering. *J. Appl. Geophys.* **2021**, *186*, 104273. [\[CrossRef\]](#)
26. Zhu, P.; Xu, X.; Ma, Z.; Wang, Y. Research on Accuracy and Error Analysis of Coal and Rock Strata Detection Based on Air-Coupled GPR. *IEEE Geosci. Remote Sens. Lett.* **2022**, *19*, 4024605. [\[CrossRef\]](#)

27. Xue, W.; Chen, K.; Li, T.; Liu, L.; Zhang, J. Efficient Underground Target Detection of Urban Roads in Ground-Penetrating Radar Images Based on Neural Networks. *Remote Sens.* **2023**, *15*, 1346. [[CrossRef](#)]
28. Sengani, F. The use of ground Penetrating Radar to distinguish between seismic and non-seismic hazards in hard rock mining. *Tunn. Undergr. Space Technol.* **2020**, *103*, 103470. [[CrossRef](#)]
29. Moradi, B.; Fernández-García, R.; Gali, I.G. E-Textile Metamaterials: Stop Band Pass Filter. *Appl. Sci.* **2021**, *11*, 10930. [[CrossRef](#)]
30. Tomassi, A.; Milli, S.; Tentori, D. Synthetic seismic forward modeling of a high-frequency depositional sequence: The example of the Tiber depositional sequence (Central Italy). *Mar. Pet. Geol.* **2024**, *160*, 106624. [[CrossRef](#)]
31. Omar, Y.M.; Plapper, P. A Survey of Information Entropy Metrics for Complex Networks. *Entropy* **2020**, *22*, 1417. [[CrossRef](#)] [[PubMed](#)]
32. Liu, Y.; Irving, J.; Holliger, K. Weighted Diffraction-Based Migration Velocity Analysis of Common-Offset GPR Reflection Data. *IEEE Trans. Geosci. Remote Sens.* **2023**, *61*, 5901509. [[CrossRef](#)]
33. Salucci, M.; Poli, L.; Massa, A. Advanced multi-frequency GPR data processing for non-linear deterministic imaging. *Signal Process.* **2017**, *132*, 306–318. [[CrossRef](#)]

Disclaimer/Publisher’s Note: The statements, opinions and data contained in all publications are solely those of the individual author(s) and contributor(s) and not of MDPI and/or the editor(s). MDPI and/or the editor(s) disclaim responsibility for any injury to people or property resulting from any ideas, methods, instructions or products referred to in the content.